Rev. Roum. Sci. Techn.– Électrotechn. et Énerg.
Vol. **67**, *1*, pp. 439–444, Bucarest, 2022

MICROSTRUCTURE AND ELECTRICAL PROPERTIES OF CACO3-DOPED ZNO– (BI2O3, SB2O3) BASED VARISTOR CERAMICS

FAIÇAL KHARCHOUCHE[1], ABDELKARIM ZEBAR[2]

Keywords: Varistor; $CaCO_3$ doped- ZnO; Bi_2O_3; Sb_2O_3; Microstructure; Nonlinear coefficient.

In this study, varistors based on ZnO were developed according to this composition, where the varistors based on 0.5% Bi_2O_3 / 0.5 % Sb_2O_3 / 99 % ZnO doped with 1 % molar, 2 % molar, and 4% molar $CaCO_3$ all samples are prepared by the conventional ceramic method, the samples were sintered at a fixed temperature of 1000 °C in the air for two hours. To see the influence of $CaCO_3$ on the additive, the microstructure and the densification behavior have been considered, and the electrical properties of the ZnO varistor ceramics have been studied. The average grain size is measured and determined. The crystallinity of the samples was determined. It was seen that the increase in the quantity of $CaCO_3$ slightly decreased the relative density of the sintered pellets in the range of 98.2 to 97.2 %, and the average size of the grains increased slightly in the range of 1.75 to 2.89 µm. The union of $CaCO_3$ markedly increased the breakdown field from 83 to more than 1000 V/mm. The sample with 4 mol % $CaCO_3$ had the highest nonlinear coefficient, and the sample without $CaCO_3$ had the lowest. Moreover, the relative density and the leakage current (I_L) decreased with the amount of $CaCO_3$.

1. INTRODUCTION

Varistors are electrical elements that have variable resistivities depending on the electric field, which is used for protection against overvoltages, allowing to avoid the propagation of these electrical disturbances in a system (*e.g.*, electrical network or electronic circuit): mounted in parallel with the circuit to be protected, this type of component allows limiting the effect of overvoltages without impacting the operation of the system to be protected [1,2]. The main characteristic of varistors is their variable electrical conductivity, depending on the voltage applied to their terminals: very insulating at low voltage, varistors become very conductive above their transition voltage, called "threshold voltage". The extraordinary physical and chemical properties of zinc oxide have made it the providential candidate that can significantly improve the quality of many components and, even more so, the varistor effect. ZnO has already been tested with microcrystalline materials and has given some satisfaction; it has a variable resistance, a high coefficient of nonlinearity [1–3], and a low loss under operating voltage. Many zinc oxide-based varistors on the market are used as lightning arresters [3,4]. This is formed at about 98% by moles of ZnO. The remaining 2 % corresponds to additives. The choice of the optimal chemical compositions leads to the development of varistors with a high non-linearity coefficient resulting essentially from empirical work requiring quantities of experimental plans. The addition of oxides metal influences the electrical characteristics and/or the microstructure of the final material developed during production or shaping. We give in the following paragraphs the main constituents encountered in the varistors through their effects on the material's properties and their role in elaboration. The conditions for the enhancement of varistors based on ZnO have the subject of much research to lead to the implementation of manufacturing processes optimal. The addition of cobalt and manganese decreases the interstitial zinc concentration in the zinc oxide; this decrease leads of the number of donor defects, therefore of the density of charge carriers and thus decreases the conductivity [4,5]. Varistors in this day exhibit high non-linear current-voltage characteristics. They are the most time-consuming produced by sintering a mixture of ZnO powders considered a matrix with weak quantities of other metal oxides like SnO_2, Bi_2O_3, TiO_2, $SrTiO_3$, $BaTiO_3$, Sb_2O_3, WO_3 or even CeO_2 [4–9]. The choice of these oxides is their wide bandgap semiconductor character ($Eg > 3$ eV). The nonlinear current-voltage electrical characteristic of ceramic zinc oxide-based varistors is due to the formation of double Schottky barriers at the grain boundaries. Preparation of commercial ZnO-Bi_2O_3 varistors by the classical method. However, this method is difficult to control with high precision, resulting in desirable grain microstructure and electrical characteristics. For this, several studies have been set up to know the effect of certain dopants like Ce_2O_3, Ho_2O_3, La_2O_3, Dy_2O_3, Y_2O_3, *etc.*, on the increase in grain size or the control of the microstructure of ZnO-based varistors as well as the electrical characteristics [7–14]. Varistor formulations, the most common, contain bismuth and antimony oxides; these form with zinc oxide, the spinel $Zn_7Sb_2O_{12}$, and pyrochlore $Bi_3Zn_2Sb_3O_{14}$ phases, as well as several bismuth-rich phases. These phases are generally located in the intergranular zones. Zinc oxide-based varistors exhibit semiconductor and nonlinear properties. The non-linearity coefficient (α) is high since it is around 40, *i.e.*, the usual value of commercial varistors. Many nonlinear systems exist, such as SiC, $SrTiO_3$, TiO_2, WO_3, *etc*. [2,3,8,11–14]. These materials have nonlinearity coefficients that are always less than 20 and are, therefore, unsuitable for electrotechnical applications such as medium voltage surge arresters [1,3,13]. In this work, the preparation of Sb_2O_3 /Bi_2O_3/ZnO -based varistor ceramics using a classic ceramic procedure at a temperature of 1000 °C was studied across the effect of $CaCO_3$ addition on varistors microstructure and the sintering behavior of the system. Relative density, grain size, and the current density (J)-electric field (E) characteristics were measured at room temperature using a low-voltage source-measure unit (Keithley Model 237) to obtain a non-linear coefficient (α).

[1] DAC-hr Laboratory, Electrical engineering department, University of Ferhat Abbas Setif 1 , Setif, Algeria, Kharchouche.electro@yahoo.fr.
[2] QUERE laboratory, Electrical engineering department, University of Ferhat Abbas Setif 1, Setif, Algeria, zebarkarim@yahoo.fr.

2. EXPERIMENTAL PROCEDURE

In the case of this study, we chose a high-purity nano-ZnO powder (Nanogard, 99.99 % purity, average particle size 60 nm). Standard proportions of additives such as Bi_2O_3 and Sb_2O_3 powder have been incorporated with zinc oxide powder as shown in this formula of 99 % ZnO + 0.5 % Bi_2O_3 + 0.5% Sb_2O_3 (all in mol%). Subsequently, pure powdered $CaCO_3$ (1, 2, and 4 mol%) was used in the preparation of four samples, where the basic composition was the following system 99 % ZnO + 0.5 % Bi_2O_3 + 0.5 % Sb_2O_3 + X mol% $CaCO_3$ (ZBS+ Xmol% $CaCO_3$). The formula for each sample is abbreviated as follows Z0 (ZBS), Z1 (ZBS + 01mol % $CaCO_3$), Z2 (ZBS + 02mol % $CaCO_3$), and Z3 (ZBS + 04 mol % $CaCO_3$), the experimental protocol for the elaboration of our varistors have been made by the classic way of mixing oxide. Selected powders are mixed in small amounts (~50 g), in deionized water with zirconia beads and ethanol, in polypropylene vials filled with 5 mm diameter zirconia beads using a mixer. The mixing time is about 2 hours. The balls promote the homogenization of the mixture but are not there to grind the powders. The low rotation speeds (2 rev/min) also prevent pollution of the mixture by debris from zirconia beads. The powders are then dried in an oven at 110° C. for 12 hours. The powders then undergo calcination in a superkhantal Linn air oven with isothermal maintenance at 800 °C for 2 hours (rise ramp of 10 °C·min^{-1}).

However, the recovered powder mixture is ground in a mortar and sieved through a 200 μm sieve. Shaping by pressing requires the powder to have a certain cohesion allowing it to be obtained from compact discs pressed from 0.5 g of powder. For this, we added to the powder an organic binder based on a mixture of polyvinyl alcohols (PVA), diluted in an aqueous medium at 4% by weight which promotes the raw mechanical strength of the pressed samples.

The binder coats the grains to form a thin plastic layer, forming so-called 'soft' easily deformable agglomerates, which help the arrangement of the particles during pressing. The incorporation is done in a porcelain mortar at the rate of two drops for a batch of 10 g of powder to have a paste. The latter is dried at 80 °C in an oven for one hour, then recovered, crushed in a mortar, and sieved through a 200 μm sieve. Our technique consists of getting in shape the initial powder. Two complementary compression protocols were implemented: uniaxial compression (on a Sodemi RD20E press equipped with a cylindrical die) at sufficient pressure to ensure the cohesion of the compact, followed by cold isostatic compression at higher pressure (Cold isostatic press, 4000 bar, 15x15x20, Novassis). Maximum pressure of 40 MPa is reached with uniaxial pressing. Beyond this pressure, the samples are cracked.

The isostatic pressure reached is 300 MPa for 5 min. This forming generally makes it possible to reach relative densities when raw (before sintering) of the order of 60 to 70 % of the theoretical density of the material. The dimensions of the cylindrical compacts prepared by pressing are close to 8 mm in diameter and 1.5 mm thick. Sintering was performed at 1000 °C for 2 h with a heating and cooling rate of 5 °C/min in a programmable oven for all samples. The Archimedes method was applied to determine the density of the samples. To highlight and understand the microstructural modifications induced by densification and better control the microstructural evolutions to optimize the electrical and dielectric properties, the four samples were characterized by high-resolution scanning electron microscopy and mapping. Energy dispersive X-ray analyzer (EDX) (Hitachi S-3500N). X-ray powder diffraction pattern was recorded on a Rigaku D/MAX-2200 diffractometer using Cu K radiation. X-ray diffraction analysis (XRD) (RU-200, Rigaku Co. Ltd) also identified the sample's crystalline phase. The grain size was measured using the intercepted segment method (linear interception) [4,5,15].

This method's principle consists of tracing several segments of length L on the micrograph to be characterized and counting the number N of grains intercepted. Grains not entirely cut are counted as half a grain. To ensure a better contact with the electrodes (measuring device), the pellets are metalized using a thin layer of silver paste on both sides of the pellet, followed by annealing in an oven conventional, at 650 °C for 10 min. The diameter size of the electrodes was 10 mm. The size of the electrodes was 10 mm in diameter.

After this step, we placed each sample between the electrodes to measure and justify the electrical characteristics of the samples. The current/voltage characteristic was obtained using a voltage source equipped with a nano-ammeter (Keithley 237, measure source unit) at room temperature. In contrast, the nonlinear coefficient α was calculated from the following equation,

$$\alpha = \frac{\text{Log } J_2 - \text{Log } J_1}{\text{Log } E_2 - \text{Log } E_1}. \quad (1)$$

with J_1 and J_2 equal 1 mA·cm^{-2} and 10 mA·cm$^{-2,}$ respectively. where E_1 and E_2 are the electric fields corresponding to J_1 and J_2, respectively. The breakdown field (E_{1mA}) was measured at 1.0 mA·cm^{-2} in the current density, and the leakage current density (J_L) was measured at 0.8 E_{1mA}. The final diameter of the samples was 8 mm and 1.0 mm in thickness.

3. RESULTS AND DISCUSSION

Observing the surface or the morphology of zinc oxide powders by scanning electron microscopy (SEM) allows both to verify the grain size and the shape of the grains. SEM characterizes the ZnO powders obtained; the corresponding images are shown in Fig. 1, a similar morphology consisting of large aggregates agglomerated between them.

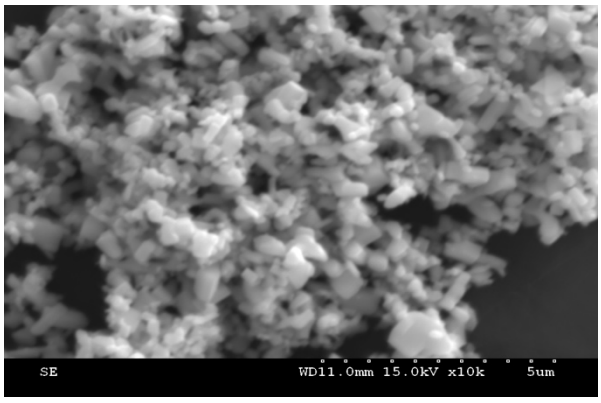

Fig. 1 – SEM image of ZnO powder.

These aggregates are made up of nanoparticles and microparticles, and the particle size of ZnO varies from 100 nm to 1.5 μm.

According to the mode used in this work, we could perform an elemental analysis at a specific point (on a volume of approximately 5 μm). The results of the EDX (Fig .2, b) analysis presented in Table 8 give the elemental compositions with a high concentration of additives such as

Ca, C, Zn, Bi, Sb, and O. The distribution of the chemical elements are well dispersed in a homogeneous way for each component. EDX mapping of the elemental distribution shows that Ca is highly dispersed in the ZnO matrix

3.1. MORPHOLOGY AND STRUCTURAL PROPERTIES

3.1.1. EDX MAPPING

So, the analysis carried out by EDX makes it possible to determine the composition and distribution of the chemical elements in our analyzed sample (Bi_2O_3, Sb_2O_3)-doped ZnO-based varistor sintered at 1000 °C for two hours containing 4 mol% $CaCO_3$ (Fig 2).

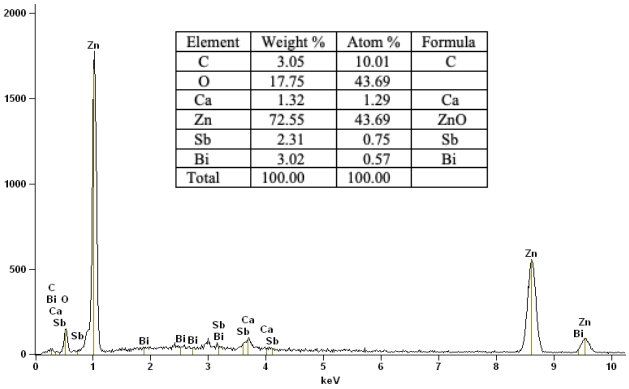

a) EDX spectrum

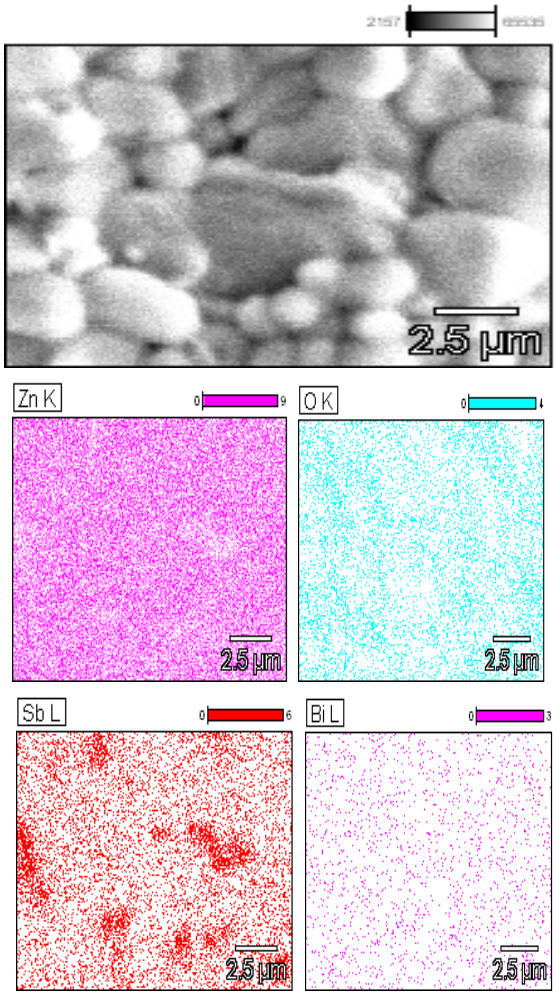

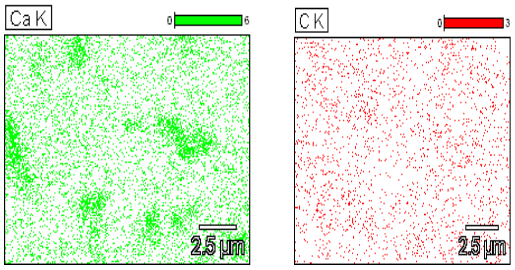

b) Morphology of the sample and EDX mapping of the elemental distribution of Zn, O, Sb, Bi, Ca, C

Fig. 2 – EDX spectrum (a) and EDX; mapping(b) of (Bi_2O_3, Sb_2O_3)-doped ZnO-based varistor sintered at 1000°C for two hours containing 4 mol% $CaCO_3$.

3.1.2. SEM OBSERVATION

Figure 3 represents the SEM micrographs of each sample after sintering at 1000◦C for two hours. At this temperature, a difference in microstructure is relatively different from the average size of ZnO grains. The data in Table 1 are explained the size of ZnO grains. The smallest size is proportional to the sample (Z0). It is seen from the micrographs of the four samples that the grain size increases with the increasing content of $CaCO_3$. The average grain size increased from 1.75 µm to 2.89 µm. The increase in grain size may result from the precipitation of the secondary phase in grain boundaries and nodal points. The size and shape of the particles of sample Z0 were different. this study shows that a bimodal microstructure of the large and fine matrix grains was noticed better in the Z0 sample. The improvement in grain size of all samples is noted in Table 1.

Table 1

The samples compositions, average ZnO grain size, and the more detailed electrical and dielectric characteristic parameters.

ZBS + Xmol% $CaCO_3$	Eb_{1mA} V/mm	$Eb_{0.1mA}$ V/mm	α	J_l mA/cm²	Grain size (µm)	Relative density (%)
Z0 (x=0)	83	33.33	2.34	0.54	1,75	98.2
Z1 (x=1)	366	33.33	1.33	0.45	2.77	97.8
Z2 (x=2)	533	283	3.69	0.45	2.77	97.5
Z3 (x=4)	X > 1000	516	9.16	0.45	2.89	97.2

The sample Z0 seems to be less porous for this. The density is a little higher than the other samples. $CaCO_3$ at 1 mol% as a dopant enhances grain size and improves microstructural uniformity. The result agrees with the one carried out in [19]. The microstructure comprises two phases: bulk phase and inter-granular phase. The SEM image of sample Z2 shows a bimodal microstructure of fine and large grains like sample Z0 with other bright fine grains). Concerning samples Z1, Z2, and Z3, the grain size is bigger than sample Z0. Their bimodal microstructure is almost similar, with grains bigger of order (0.2 – 0.3 µm) located especially in the nodal point for all the samples doped. This can be due to the high content of $CaCO_3$ (4 mol%) incorporated into the matrix. The SEM images show that the more incorporated $CaCO_3$ content is, the more the sample's porosity increases. Particle size and size distribution of powders are essential in varistor characterization. This is because they significantly affect the varistors' density and electrical properties. If the particle size distribution of the ZnO varistor is large, the rate of increase of the ZnO grain size is not the same and will lead to the reorganization of the ZnO grains. This mechanism will lead to the formation of pores in the sintered varistors [10,20,21].

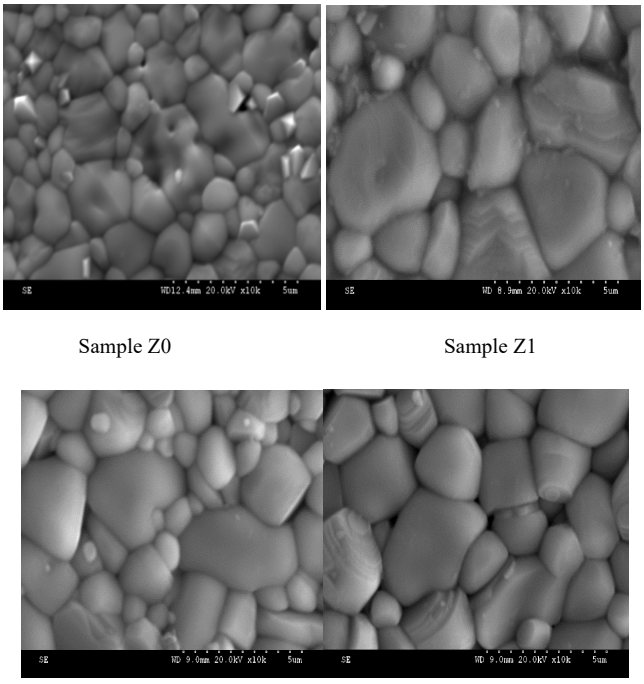

Sample Z0 Sample Z1

Sample Z2 Sample Z3

Fig. 3 – SEM micrographs of (Bi2O3, Sb2O3)-doped ZnO-based varistors and sintered at 1000 °C containing various amounts of $CaCO_3$.

3.1.3. XRD ANALYSIS

A representative XRD spectrum of the sample Z0, calcined at 800 °C, is shown in Fig. 4. The XRD study confirms the formation of a hexagonal system of ZnO. All diffraction peaks coincide with the earlier reported values, where the lattice parameters are a = 3.2495 Å and c = 5.2069 Å.

The spectrum shows a complete decomposition of organic residues at 800 °C, chosen as the calcination temperature. No impurity peaks were present within the detection limit of XRD. No preferential orientation was observed. All major peaks can be indexed as a ZnO phase according to the joint committee on powder diffraction standards (JCPDS) database (01-089-7102).

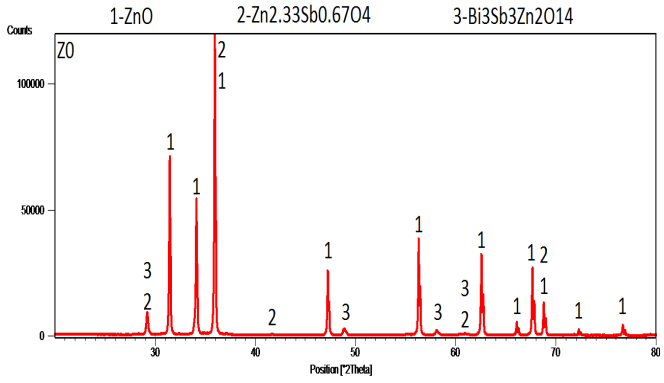

Fig. 4 – XRD patterns of the sample Z0 were calcined at 800 °C for two hours.

The spectrum of Z0 reveals that the microstructure consisted of three phases: ZnO grain (primary phase) characterized by a peak appearing at an angle of 2θ = 36.256 ° (corresponding to (101) reflection) and other solid phases, $Zn_{2.33}Sb_{0.67}O_4$ and $Bi_3Sb_3Zn_2O_{14}$ characterized by peaks appearing, respectively, at angles 2θ = 34.605° and 2θ = 29.555° and correspond, respectively, to plans reflection (311) and (222). These two solid solutions can be in the grain boundaries of ZnO.

The SEM image of Z0 (Fig. 3, a) shows only two phases: a bulk phase and an intergranular phase. The bulk phase contains large grains whose size can result from substituting additive ions in the ZnO structure. Many Bi_2O_3 and Sb_2O_3 particles were dissolved into the melt entirely during the solution-precipitation process, meaning that a strong interaction between ZnO and additive in the mixture occurred. Figure 5 shows the XRD patterns of sample Z1. The XRD patterns showed hexagonal ZnO as the major phase. The XRD showed complete decomposition of organic residues at 800 °C, chosen as the calcination temperature. The spectrum of powder of sample Z1 reveals that the microstructure consisted of three phases: ZnO grains (primary phase). All major peaks can be indexed as zinc oxide phases according to the JCPDS database (01-089-7102), characterized by a peak appearing at an angle of 2θ = 36.337° (corresponding to (101) reflection). Other phases Bi_2O_3, $ZnSb_2O_4$, Sb_2O_4, and CaO, characterized by peaks appearing, respectively, at angles 2θ = 28.835°, 2θ = 27,858°, 2θ = 29,063°, 2θ = 34,467° and 2θ = 37,361° and correspond, respectively, to (410), (112), (211), (220) and (002) refection plans. The densities of calcination of different phases are closer to that of the samples Z0 and Z_1.

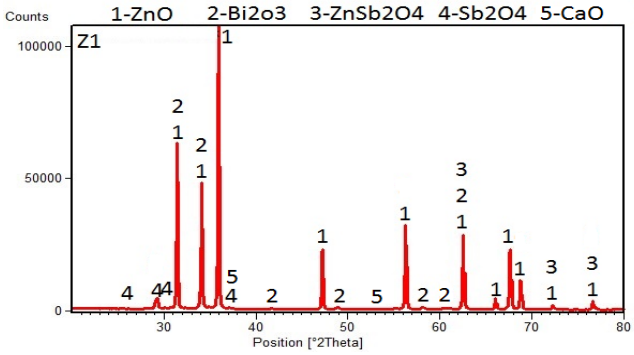

Fig. 5 – XRD patterns of $CaCO_3$-doped varistor powders were calcined at 800 °C for two hours.

3.2. ELECTRICAL PROPERTIES

Figure 6 shows the electric field-current density (E-J) characteristics of the samples modified with various additives.

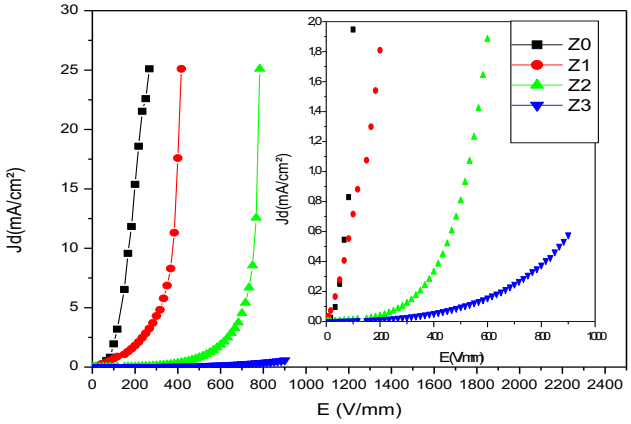

Fig. 6 – J-E characteristic for 1000°C as sintering temperature

The curves show noticeable varistor properties that show a nonohmic character in the E-J measurements. The

characteristics of the varistors consisted of two piecewise linear regions near the knee. A sharper knee between the two regions will result in better non-ohmic properties. The breakdown electric field noticeably increased from 83 to 533 when $CaCO_3$ increased from 0 to 3 mol% $CaCO_3$ with a firing temperature of 1000 °C. Hence, $CaCO_3$ significantly affects the breakdown, grain size, and grain boundaries at 1000 °C, as specified in Table 1.

Table 1

The samples compositions, average ZnO grain size, and the more detailed electrical and dielectric characteristic parameters are summarized

ZBS + Xmol% $CaCO_3$	Eb_{1mA} V/mm	$Eb_{0.1mA}$ V/mm	α	J_I mA/cm²	Grain size (μm)	Relative density (%)
Z0 (x=0)	83	33.33	2.34	0.54	1,75	98.2
Z1 (x=1)	366	33.33	1.33	0.45	2.77	97.8
Z2 (x=2)	533	283	3.69	0.45	2.77	97.5
Z3 (x=4)	X > 1000	516	9.16	0.45	2.89	97.2

The coefficient of non-linearity (α) follows the behavior of the breakdown electric field as a function of the $CaCO_3$ content and firing temperature. It is observed that the increase of the content of $CaCO_3$ improves (increases) the nonlinear coefficient.

When increasing $CaCO_3$ contents between 0 mol% and 4mol%, the threshold voltage is more than that of the original composition, while the threshold voltage increases when increasing the content of $CaCO_3$. The result corresponds effectively to the evolution of the grains' size since breakdown voltage increases when the average grains size decreases. Therefore, the samples elaborated in this work can be used as high voltage varistors with compact sizes. The following expression can explain the behavior of E_{1mA} following CaCO3 content:

$$E_{1mA}=\frac{vgb}{d}, \tag{2}$$

where d is the average grain size, and v_{gb} is the breakdown voltage per grain boundaries. This expression indicates that the d and v_{gb} values directly determine E_{1mA}. The E_{1mA} is affected, on the one hand, by the increase in the number of grain boundaries was influenced by the decrease in the size of the ZnO grains, and on the other hand, by the increase of breakdown voltage per grain boundaries, by the increase of breakdown voltage per grain boundaries. This system is more strongly affected by v_{gb} than average grain size decreasing in the small range with an increase in the content of $CaCO_3$.

The curves show that the conduction characteristics divide into two regions. In the first part of the curve and before the breakdown field, the current does not almost flow as a function of the field. In the second part of the curve, after the breakdown field, the current abruptly increases with the increasing electric field. Overall, the voltage-current relation is nonlinear. The sharper the knee of the curves between the two regions, whereas it determines the non-linearity coefficient α. Greater is α, the better the non-linearity of the varistor. The coefficient (α) of the varistor Z0 (without $CaCO_3$) is only 2.34, whereas the values (α) of the samples (Z1, Z2, and Z3) are in the range of 1.39 – 9.16. The detailed electrical parameters are summarized in Table 1. All the samples provide a high voltage, whereas the E_{1mA} values range 83-533 V/mm.

4. CONCLUSION

After the preparation of the samples by the conventional method, it was possible to obtain varistors based on ZnO doped with some CaCO3 content with percentages varying between 1 mol% up to 4 mol%. EDX has investigated the microstructural study, electrical characterization, SEM, and a V–I source/measure unit well.

In this work, 1000°C was the choice as sintering temperature. The results are summarized as follows.

- The calculations, at 800 °C of the sample Z0 (without $CaCO_3$), form $Zn_{2.33}Sb_{0.67}O_4$ and $Bi_3Sb_3Zn_2O_{14}$ as a solid solution in addition of the phase ZnO. Sb and Bi oxides are dissolved in the grain core, whereas the grain size increases.
- The calculations, at 800 °C of the sample Z1 (containing 1 mol% $CaCO_3$), show that the sample consisted of various phases such as ZnO grain as the main phase, and Bi_2O_3, $ZnSb_2O_4$, Sb_2O_4, and CaO as a solid solution in addition to the phase ZnO and as secondary phases.
- The sintered densities of the doped samples also decreased from 98.2 % to 97.2 % to a small extent with increasing $CaCO_3$ amount.

Both the morphology and the microstructure of the sample fabricated under the optimum conditions were studied by SEM. As can be seen, the grains were uniform and well distributed throughout the sample's microstructure with a high relative density.

- From EDX analysis, the Ca, C, Bi, Sb, and O were found at the grain's boundaries

The electrical properties analyzed illustrate those values of the nonlinear coefficient of the varistor ceramics are 1.33–9.16, the sample doped with 4 mol% $CaCO_3$ exhibited good non-ohmic properties: 9.16 in the nonlinear coefficient, and 0.45 mA/cm^2 in the leakage current density. All the samples provide a high voltage, whereas the E_{1mA} values are 83-533 V/mm, and the leakage current is 0.54–0.45 mA/cm^2.

- The grain size of the samples decreases significantly, from 1.75 to 2.89 μm, with increasing $CaCO_3$ concentration. The relative density and I_L decrease with increasing $CaCO_3$ concentration.

According to this study, it was noticed that the increase in the amount of $CaCO_3$ addition gave an improvement in the electrical behavior of the varistors. The results obtained show that the varistors are suitable for low-voltage applications. However, an increasing number of low voltage varistors are used for overvoltage protection in integrated circuits, automobiles, machinery, and equipment, as well as electronic components, boards, and chips.

ACKNOWLEDGMENT

The authors would like to express gratitude and acknowledgment to the research laboratories of the University Ferhat Abbes Setif 1 and the laboratory director LMCPA and her team, the University of Valenciennes, for their help

Received on 23 August 2022

REFERENCES

1. A.S. Tonkoshkur, A.B. Glot, A.V. *Ivanchenko, Percolation effects in dc degradation of ZnO varistors*, J. Adv. Dielect., **5**, *1*, pp. 1550008–8 (2015).
2. F. Munteanu, F.M. Frigura-Iliasa, E. Cazacu, A.t Establishing, *The Functional Limits Of A Zno Varistor Based Surge-Arrester*, Roum. Sci. Techn.– Électrotechn. et Énerg., **52**, **4**, pp. 443–452 (2007).
3. D.R. Clarke. *Microstructural location of intergranular metal oxide phase in a zinc-oxide varistor*, Journal of Applied Physics, **49**, *4*, pp. 2407–2411 (1978).
4. T. Mandal, P. Mandal, P. Mondal, L. Murmu. *Design of dual band monopole antenna for bluetooth and ultra wide bandwith triple notch using electromagnetic bandgap structure,* Roum. Sci. Techn.– Électrotechn. et Énerg., **67**, *3*, pp. 307–312 (2022).
5. L.T. Mei, H.I. Hsiang, C.S. Hsi, F.S. Yen, *Na_2CO_3 Doping Effect on ZnO-Pr_6O_{11}-Co_3O_4 Ceramic Varistor* Properties, Journal of Alloys and Compounds, **558**, pp. 84–90 (2013).
6. D. Szwagierczak, J. Kulawik, A. Skwarek, *Influence of processing on microstructure and electrical characteristics of multilayer varistors*, Journal of Advanced Ceramics, **8**, *3*, pp. 408–417 (2019).
7. I. Baran, C. Marian, T. Leonida, C.M. Micu, *Lightning performance of high voltage overhead lines assessed using the critical currents curves*, Roum. Sci. Techn.– Électrotechn. Et Énerg., **65**, *3–4*, pp. 191–198 (2020).
8. D. Xu et al. *The Preparation and Electrical Properties of $SrTiO_3$-Based Capacitor-Varistor Double-Function Ceramics*, J. Eur. Ceram. Soc. 29, 9, pp. 1789–1794 (2009)
9. M. Lei, S. Li, X. Jiao, J. Li, M.A. Alim, *The influence of CeO_2 on the microstructure and electrical behaviour of ZnO-Bi_2O_3 based varistors*, Journal of Physics D: Applied Physics, **37**, pp. 804-812 (2004).
10. F. Kharchouche, *Effect of sintering temperature on microstructure and electrical properties of ZnO-0.5 mol%V_2O_5-0.5 mol%Cr_2O_3 varistors*. J Mater Sci: Mater Electron **29**, pp. 3891–3897 (2018).
11. L.F. García, F. Azough, G. Parsons, et al., *Optimising the performance of SiC-based varistors through composition and microstructure control*, Journal of the European Ceramic Society, **42**, *2*, pp. 600-607 (2022).
12. C.C. Zhang, Y.X. Hu, W.Z. Lu, et al. *Influence of TiO_2/Sb_2O_3 ratio on ZnO varistor ceramics*. Journal of the European Ceramic Society, **22**, *1*, pp. 61–65 (2002).
13. M. Matsuoka, T. Masuyama, Y. Iida, *Voltage Nonlinearity of Zinc Oxide Ceramics Doped with Alkali Earth Metal Oxide*. Japanese Journal of Applied Physics, **8**, *10*, pp. 1275–1276 (1969).
14. S. Bernik, S. Macek, A. Bui, *Microstructural and electrical characteristics of Y_2O_3-doped ZnO–Bi_2O_3-based varistor ceramics*, Journal of the European Ceramic Society, **21**, *10*, pp. 1875–1878 (2001).
15. C.W. Nahm, *Effect of sintering time on varistors properties of Dy_2O_3-doped ZnO–Pr_6O_{11}-based ceramics*. Materials Letters, **58**, *26*, pp. 3297–3300 (2004).
16. L.C. Sletson, M.E. Potter, M.A. Alim, *Influence of sintering temperature on intrinsic trapping in zinc oxide-based varistors*, Journal of the American Ceramic Society, **71**, *11*, pp. 909–913 (1988).
17. J.A.A. Martínez, M.B. Hernández, J. Hernández, et al., *Microstructure and electrical properties in SnO_2 ceramics with sequential addition of Co, Sb and Ca*. Journal of Physics D Applied Physics, **40**, *22*, pp. 7097–7102 (2007).
18. H. Chen, L. Zheng, J. Zeng, G. Li, *Effect of Sr doping on nonlinear current–voltage properties of ZnO-based ceramics*, Journal of Electronic Materials, **50**, pp. 4096–4103 (2021).
19. W. Water, Yin-Shiang Yan, *Characteristics of strontium-doped ZnO films on love wave filter application*s, Thin Solid Films, **515**, *17*, pp. 6992–6996 (2007).
20. C.W. Nahm, *Major effect on electrical properties and aging behavior of ZnO–Pr_6O_{11}-based varistor ceramics with small In_2O_3 doping changes*, Journal of Materials Science: Materials in Electronics, **23**, pp. 1715–1721 (2012).
21. E. Manta, E.A. Patroi, D. Patroi, A. Iorga, G. Sbarcea, A. Petre, *Processing, Microstructure And Magnetic Properties Of Alnico Ribbons*, Rev. Roum. Sci. Techn.– Électrotechn. et Énerg. **66,** *1*, pp. 3–7 (2021).